Fully analytical description of adiabatic compression in dissipative polaritonic structures

Remo Proietti Zaccaria,[1,2,*] Alessandro Alabastri,[1] Francesco De Angelis,[1] Gobind Das,[1] Carlo Liberale,[1] Andrea Toma,[1] Andrea Giugni,[1] Luca Razzari,[1] Mario Malerba,[1] Hong Bo Sun,[2] and Enzo Di Fabrizio[1,3]

[1]*Italian Institute of Technology (IIT), NanoBioScience Laboratory, via Morego 30, 16163 Genova, Italy*

[2]*LaSuN, State Key Laboratory on Integrated Opto-electronics, College of Electronic Science and Engineering, Jilin University, Changchun 130023, People's Republic of China*

[3]*BIONEM Laboratory, University of Magna Graecia, Campus S. Venuta, Germaneto, viale Europa, I88100 Catanzaro, Italy*

(Received 13 February 2012; published 5 July 2012)

We have theoretically modeled and experimentally fabricated a nanoscale adiabatic (conical) metallic structure that is suitable for high-resolution Raman spectroscopy. We report on a fully complex analytical description of the adiabatic compression phenomenon which is investigated in terms of both geometrical and optical parameters. An explicit analytical description of adiabatic compression is provided together with the physical role played by the complex effective refractive index of the polaritonic adiabatic mode. In particular, we have examined the role of absorption on the field enhancement. Finally, we demonstrate how such a device can experimentally enhance the Raman signal coming from nanosamples such as a bead of SiO_x and a monolayer of benzenethiol.

DOI: 10.1103/PhysRevB.86.035410 PACS number(s): 78.67.−n, 68.37.−d, 73.20.Mf, 78.30.−j

I. INTRODUCTION

In the last decade the concept of a nanodevice or nanostructure has assumed a broader meaning and its physical content, together with the spatial confinement, includes also optoelectric transport and magnetic properties. This is the consequence of an enormous effort which sees scientists around the world with the common goal of solving new kinds of emerging problems, and new device designs, all at the nanoscale level. Here we analyze a conical metallic nanostructure[1–6] with the purpose of measuring the Raman signal with nanometric resolution.[7–10] In particular, we will focus on surface plasmon polaritons enhanced Raman scattering (SPPERS). The present definition differs from the standard and well-established surface enhanced Raman spectroscopy (SERS)[11–13] and tip enhanced Raman spectroscopy (TERS)[14] because of the device structure[15] and the involved measurements. We have faced the problem both from a theoretical and fabricative point of view. The high quality of the fabricated structure provides an ideal experimental model, which is suitable for an accurate comparison with theoretical results. The structure, having the form of an almost perfect cone with a small apical angle, shows an extremely high field at its apex, namely some orders of magnitude higher than the source. This effect is the result of a phenomenon known as adiabatic compression,[2] which describes the slowing down of polaritonic waves while proceeding on the surface of a metallic cone toward the tip with contemporary increase of the field intensity. The present approach to the complete dispersion characterization of the involved materials (i.e., both real and imaginary parts of the dielectric function are considered) allows a detailed analytical electromagnetic analysis. In fact, besides the electric field distribution on the cone, either in spherical or Cartesian coordinates, we will also show the behavior of both the real and imaginary parts of the effective refractive index associated with the polaritonic field as a function of the distance from the cone apex, apical angle, and source wavelength. Furthermore, an analytical description of the adiabatic compression will be provided. Finally, prior the experimental analysis, the theoretical results will be summarized in the cone dispersion relation.

There are two ingredients responsible for the high field at the cone apex: first, the shape of the structure which has the effect of adiabatically transporting the signal from the base to the apex, therefore enhancing by many orders of magnitude its value; second, the material composing the cone. Here we have used silver that, in the visible range, is capable of supporting surface plasmon polaritons (SPPs), bosonic quasiparticles originating from the coupling between photons (incoming light) and plasmons (collective oscillations of free electrons on the cone).[16,17] The SPPs have the properties of existing only in the skin depth (a few tens of nanometers) of the metallic surface.

II. MODELING

The first approach was a 3D numerical calculation of the field distribution around a silver cone of height $h = 2500$ nm and base diameter $d = 300$ nm, which was analyzed with finite integration technique commercial software.[18] The optical dispersion of silver was considered in a Drude-Lorentz scheme,[19] while no spatial dispersion was taken into account.[20] The results, shown in Fig. 1, confirm both the already predicted adiabatic compression and the field enhancement.[2]

From an analytical point of view,[1] by describing an infinitely long metallic cone in spherical coordinates (r,ϕ,θ) [see inset in Fig. 2(a)] where the origin of the axis is at the cone apex ($r = 0$), we can determine the components of the electric and magnetic fields associated with the SPPs. In particular, in the following, a TM_0 mode is considered.[2] Under this condition, only the components E_r (radial), E_θ (polar), and H_ϕ (azimuthal) are not zero. Starting from the Maxwell equations written in spherical coordinates and writing E_r and E_θ in terms of H_ϕ, it can be shown that the three components of the electromagnetic field for a TM_0 mode each take two possible forms according to the condition $\theta \lessgtr \alpha$, where α is the half apical angle [see inset in Fig. 2(a)]. In particular, the general radial differential equation takes the form

$$\frac{d^2}{dr^2}R(r) + \frac{2}{r}\frac{R(r)}{dr} + \left(\frac{\epsilon_j 4\pi^2}{\lambda^2} + \frac{\eta^2}{r^2}\right)R(r) = 0, \qquad (1)$$

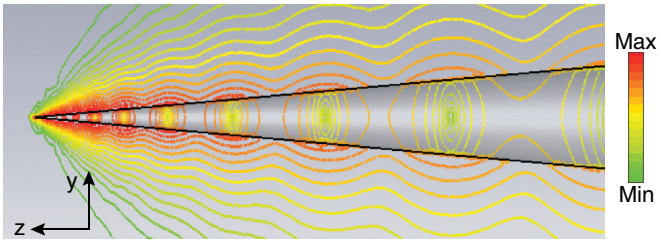

FIG. 1. (Color online) Distribution of the absolute value of the total electric field in the *YZ* plane. The chosen wavelength is $\lambda = 514$ nm. The dimensions of the silver cone are height $h = 2500$ nm and base diameter $d = 300$ nm, corresponding to an angle $\alpha = 0.06$ rad. The source is an infinitesimal dipole oriented along the axis of the cone. Brighter colors correspond to higher values of the field.

where $R(r)$ contains the radial dependence of the magnetic field H_ϕ and $\eta = \eta' + i\eta''$, in our case, is a complex separation constant connecting the radial and angular parts of the Maxwell equations written in spherical coordinates. Finally, ϵ_j is the dielectric function of either the metallic cone or the surrounding dielectric. Eq. (1) leads to a direct analytical solution under the hypothesis $\frac{\eta^2}{r^2} \gg |\epsilon_j|\frac{4\pi^2}{\lambda^2}$. In this case, and considering also the angular differential equation (not shown here) with solutions $A_1 I_0(\eta\theta)$ for $\theta < \alpha$ and $A_2 K_0(\eta\theta)$ for $\theta > \alpha$, the radial component of the electric field takes the form

$$\begin{aligned} E_{r,\theta<\alpha}(r,\theta,\eta) &= -\frac{ic}{\omega\epsilon_m}\frac{\eta A_1}{r^{3/2}} I_0(\eta\theta) 2\cos(\eta' \ln r) \\ &\quad \times (e^{\eta''\ln r} + e^{-\eta''\ln r}) e^{-i\omega t} + \text{c.c.}, \\ E_{r,\theta>\alpha}(r,\theta,\eta) &= -\frac{ic}{\omega\epsilon_d}\frac{\eta A_2}{r^{3/2}} K_0(\eta\theta) 2\cos(\eta' \ln r) \\ &\quad \times (e^{\eta''\ln r} + e^{-\eta''\ln r}) e^{-i\omega t} + \text{c.c.} \end{aligned} \tag{2}$$

Similar expressions can be written for both E_θ and H_ϕ. Here $A_{j=1,2}$ are the coefficients obtained by the continuity relation of the electromagnetic field at the interface between the metallic cone and the surrounding dielectric medium (air). Furthermore, I_0 and K_0 stand for modified Bessel functions of the first and second type, respectively. Finally, ϵ_m and ϵ_d are the complex permittivity of the metallic cone and the real dielectric function of the surrounding medium, respectively. As noted, an important aspect leading to Eq. (2) is the hypothesis that the radial coordinate r satisfies the relation $\frac{\eta^2}{r^2} \gg |\epsilon_j|\frac{4\pi^2}{\lambda^2}$. For example, the case of a silver cone with apex angle of 0.06 rad and light excitation of 514 nm leads to $r \leqslant 220$ nm. Hence, we can conclude that Eq. (2) can be used only in proximity to the tip apex (similar considerations are valid also for E_θ and H_ϕ). This approach is less general than the numerical calculation leading to Fig. 1 where a 2.5 μm long tip was analyzed; however it can provide a physical insight to the field compression. For example, we will be able to determine both the real and imaginary parts of the effective refractive index associated with the TM_0 mode which will be used to extend the definition of absorption (normally applied to flat plasmonic systems) to metallic conical structures. Furthermore, we will stress how the usual concept of absorption has to be reconsidered when dealing with plasmonic structures.

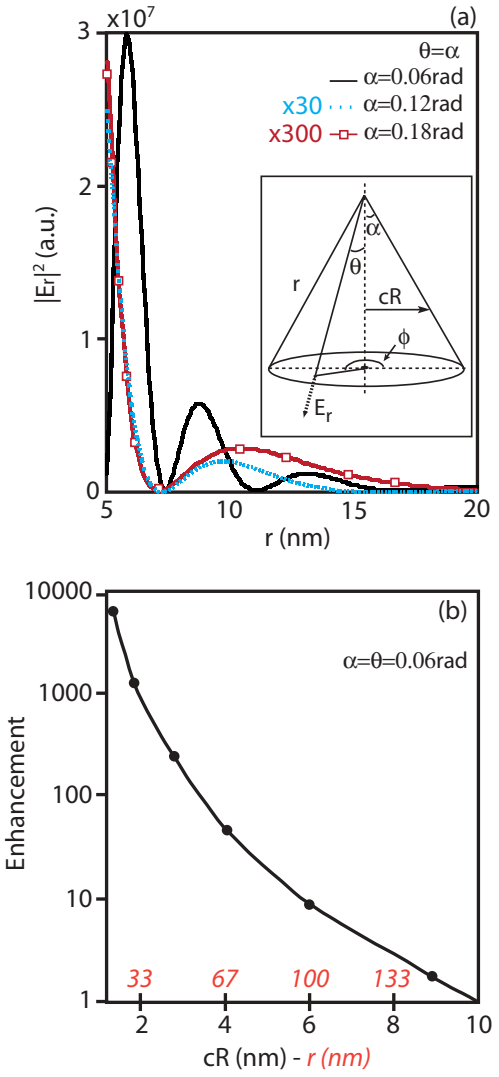

FIG. 2. (Color online) (a) Intensity associated with the component of the electric field along r for three kinds of cones identified by $\alpha = 0.06$ rad, 0.12 rad, 0.18 rad. Here $\theta = \alpha$, namely on the surface of the cone. The inset represents the geometrical model of the cone. (b) Enhancement with respect to a reference value calculated at $r = 167$ nm, namely at cone radius $cR = 10$ nm ($\theta = \alpha = 0.06$ rad). For both (a) and (b) the cone material and the wavelength of the incoming radiation are silver and 514 nm, respectively.

In order to use Eq. (2) the first step is to calculate the complex parameter η. It is possible to show that this quantity is strictly related to the values of the dielectric functions ϵ_m, ϵ_d and the angle α. Since the cone is made of dispersive material, the value of η depends on the wavelength λ of the incident light. Once η is determined, we can write A_2 in terms of A_1 from the continuity relations. Hence, the only independent variable, besides r and θ, will be A_1, which can be associated with the amplitude of the incoming light. Figure 2(a) shows the intensity associated with E_r for three cones of angles $\alpha = 0.06$ rad, 0.12 rad, and 0.18 rad, always calculated on the surface of the cones; i.e., $\theta = \alpha$. The bulk dielectric function of the silver-made cone is $\epsilon_m = -8.19 + i0.760$, corresponding to a wavelength $\lambda = 514$ nm.[19] The cone is immersed in air ($\epsilon_d = 1$). From Fig. 2(a) we can notice four

important characteristics: (1) the smaller the angle of the cone the higher the field; (2) the closer to the apex of the cone, the stronger the field; (3) the field shows alternating maxima and minima on the surface of the cone; (4) the distance between two maxima shortens approaching the cone apex (adiabatic compression). The SPP field is not a standing wave but a propagating field whose intensity increases approaching the apex as r^{-k}, where $k = 1/2,3/2$ ($E_r, E_\theta \rightarrow k = 3/2$; $H_\phi \rightarrow k = 1/2$). The effective wavelength of the surface field decreases by approaching the cone apex; that is, the phase and the group velocity tend to zero at the vertex[2] (where actually the field cannot be defined).

Aiming to provide also information on the enhancement characteristic of the metallic conical tip, we have calculated the intensity field along the surface of the cone with respect to a reference value measured at radius of the cone $cR = 10$ nm ($r = 167$ nm). This value was chosen to respect the constrains of $r \leqslant 220$ nm valid for $\lambda = 514$ nm. Furthermore, the enhancement was plotted versus both the radius of the cone cR and the radial coordinate r. This is motivated for an easy comparison with results already present in the literature.[21] Figure 2(b) shows the enhancement for a silver conical tip of angle $\alpha = 0.06$ rad and $\lambda = 514$ nm.

Figure 3 shows the distribution of $|E_r|^2$ on the plane (r,θ) for $\alpha = 0.06$ rad. It is interesting to notice that for $\theta > \alpha$ (outside the cone) the intensity rapidly decreases. Also in this case the situation is mathematically different from a flat metallic surface; in fact now the decay is determined by the behavior of the modified Bessel function of the second kind $K_0(\eta\theta)$, whereas in a flat surface the decay is exponential-like. By comparing these two mathematical expressions as done in Fig. 4, we can see that the decay originated by a conical structure is faster than the one calculated in a flat metallic surface, both in metal and dielectric. This leads to the conclusion that a conical tip represents a very good tool for generating a localized field.

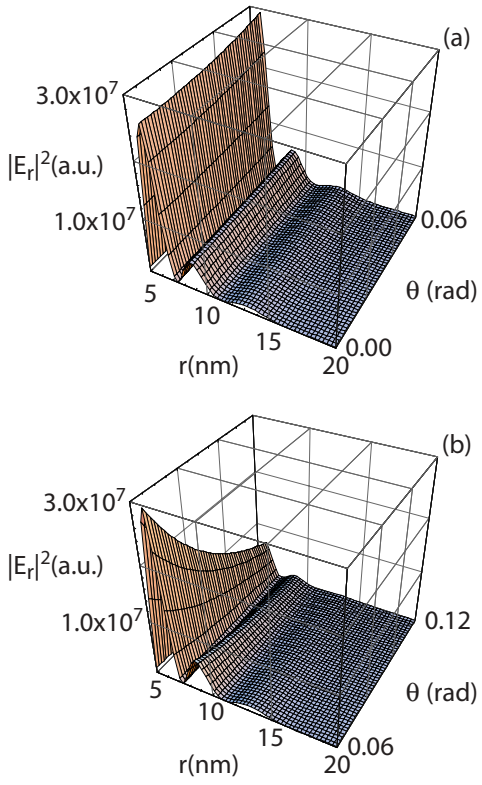

FIG. 3. (Color online) Intensity related to E_r as function of the variables r and θ with $\alpha = 0.06$ rad. (a) $\theta < \alpha$, inside the cone; (b) $\theta > \alpha$, outside the cone. For the continuity conditions of E_r at the interface, (a) and (b) provide the same intensity profile at $\theta = \alpha$ (on the cone surface). By observing the axis $\theta = \alpha$ we can see that the signal drops by two orders of magnitude at just 3 nm from the vertex.

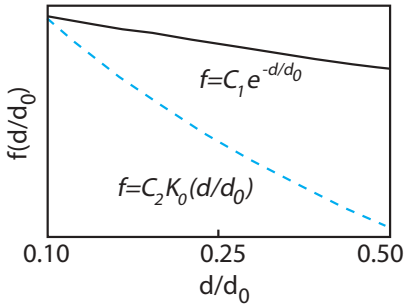

FIG. 4. (Color online) Comparison between a modified Bessel function of the second kind (K_0) and an exponential function. The former represents the decay of electric field away from a metallic conical surface, the latter from a metallic flat surface, both of them surrounded by a dielectric medium. The terms C_1 and C_2 are the matching coefficients. The horizontal axis can be read as the distance d away from the metal surface (the modified Bessel function K_0 determines the decay of E_r in the dielectric). d_0 is the length unit.

When the case $\theta < \alpha$ (inside the cone) is considered, the decay is not that rapid, at least in regions close to the vertex of the cone. As indeed shown in Eq. (2), the modified Bessel function of the first kind $I_0(\eta\theta)$ has the characteristic to remain different from zero also for θ equal to zero. This means that along the axis of the cone, the electromagnetic field will never be null [see Fig. 3(a)]. This behavior is however related to the fact that Eq. (2) is valid in the regime of small r, namely in the spatial region where the metallic cone is not thick enough to attenuate the electric field.

III. ADIABATIC COMPRESSION AND EFFECTIVE REFRACTIVE INDEX

Additional information, accompanied by a more intuitive way of observing the behavior of the electromagnetic field in the domain around the conical tip, can be obtained by means of a Cartesian coordinates plot, as shown in Fig. 5. The intensity of the total electric field is plotted in logarithmic scale along the axis out of the figure plane for a better identification of the intensity nodes. The figure shows very clearly the shortening of the wavelength by approaching the tip apex (adiabatic compression), which is related to the increase of the real part of the effective refractive index. Figure 6 quantifies this behavior by showing the effective refractive index associated with the surface plasmon polaritons. Three curves are plotted, corresponding to three different values of the angle α. For smaller angles, both the real and imaginary parts of the effective refractive index are higher, namely the sharper the cone the stronger is the field and smaller the

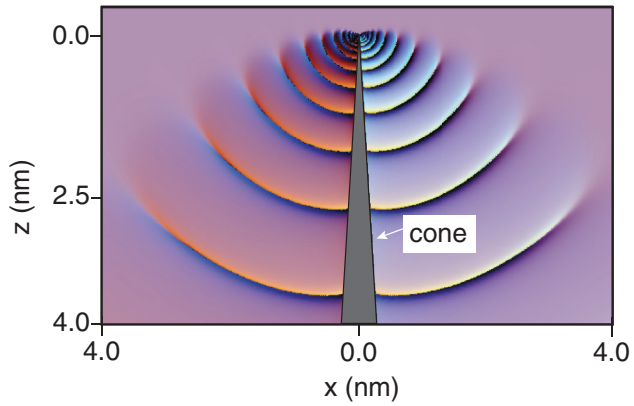

FIG. 5. (Color online) Total electric field intensity for $\theta > \alpha$. The plot is in logarithmic scale for the direction out of the figure plane. Both the vertical and horizontal axis represent lengths, with nm units. The cone is at the center of the figure. The effective wavelength compression toward the cone apex is well illustrated in the figure.

mode velocity. In particular, the expression of the effective refractive index $n_{\text{eff}} = n'_{\text{eff}} + in''_{\text{eff}}$ is related to the complex parameter η by the expression $n_{\text{eff}} = \frac{c\eta}{\omega r}$. It is useful to notice that $n_{\text{eff}}(\alpha,r) = l \times n_{\text{eff}}(l \times \alpha,r)$, where l is a real positive number, is valid in Fig. 6. This is a direct consequence of the

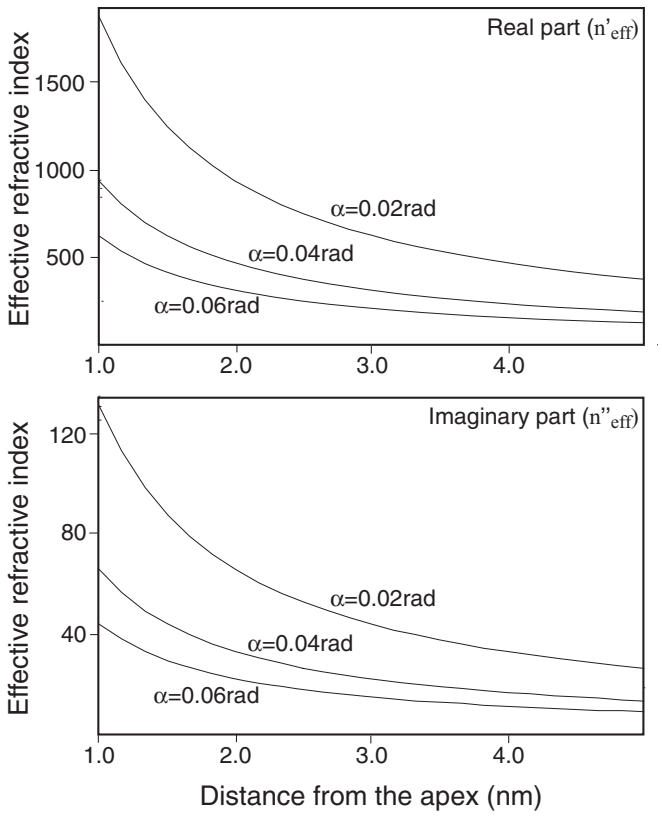

FIG. 6. Real and imaginary parts of effective refractive index experienced by the SPP versus distance calculated from the tip apex for three different values of α: 0.06 rad, 0.04 rad, and 0.02 rad. The smaller is α, the higher is the effective refractive index at a given distance from the tip apex. The incoming radiation has a wavelength $\lambda = 514$ nm.

dependence of the parameter η on the apex angle α [which can be shown to be $\eta(\alpha) = l \times \eta(l \times \alpha)$].

One of the most important characteristics associated with a TM_0 mode in a metallic conical structure is its adiabatic behavior. We shall discuss this aspect in details which will become useful for a later comparison with the field on a metallic flat surface. We have seen that the differential equation dictating the radial behavior of the H_ϕ component of the TM_0 mode is

$$\frac{d^2}{dr^2}R(r) + \frac{2}{r}\frac{R(r)}{dr} + \frac{\eta^2}{r^2}R(r) = 0.$$

Its solution has the form

$$R(r) = r^{-1/2}\left(r^{-\sqrt{1/4-\eta^2}} + r^{+\sqrt{1/4-\eta^2}}\right).$$

When its complex conjugate is considered [in order to produce a real function $R(r)$] and by assuming $\eta = \eta' + i\eta''$ with $|\eta'| \gg |\eta''|$ the previous equation becomes

$$\begin{aligned} R(r) &= r^{-1/2}2\cos(\eta' \ln r)(e^{\eta'' \ln r} + e^{-\eta'' \ln r}) \\ &= r^{-1/2}4\cos(\eta' \ln r)\cosh(\eta'' \ln r). \end{aligned} \tag{3}$$

This expression is the analytical representation of the adiabatic behavior as in Fig. 2(a). In particular, the cosine contains the zeros of the function and the exponential part assures an overall increase of the field. Furthermore, the higher η' the higher is the zeros' density and, similarly, the higher η'' the stronger is the field. This last intriguing consequence will now be discussed.

IV. ABSORPTION OF SURFACE PLASMON POLARITONS IN CONICAL METALLIC STRUCTURES

In the previous sections we have seen how the polaritonic field can be strongly influenced by the geometrical properties of the conical structure. Here we will see the dependence associated with the source wavelength. Figure 7(a) plots the behavior of the real part of the effective refractive index versus the distance from the cone tip when three different wavelengths, $\lambda = 514$ nm, $\lambda = 600$ nm, and $\lambda = 700$ nm, are evaluated. A similar plot, but for the imaginary part of the refractive index, is provided in Fig. 7(b). The graphs show that an increase of the wavelength of the incoming radiation implies a reduction of both the real and imaginary parts of the effective refractive index.

By considering the standard definition of propagation length, namely the distance reducing the field intensity by a factor e, the expressions of effective refractive indexes can be used for the calculation of what we introduce as the *quasi*-absorption (QA) of a TM_0 mode along a metallic cone. The prefix *quasi* arises from the fact that we have been considering an adiabatic system which inherently implies an increase of the field toward the tip; hence the standard definition of absorption cannot be applied to the present system. However, we can suppose that the amplitude of the field at different wavelengths λ is proportional to the QA of the field itself.

Before entering in the analysis of the QA associated with a metallic conical structure, it is convenient to recall the optical behavior of surface plasmon polaritons along a flat metallic-dielectric interface. In fact, the mathematical expression describing the surface decay on this kind of

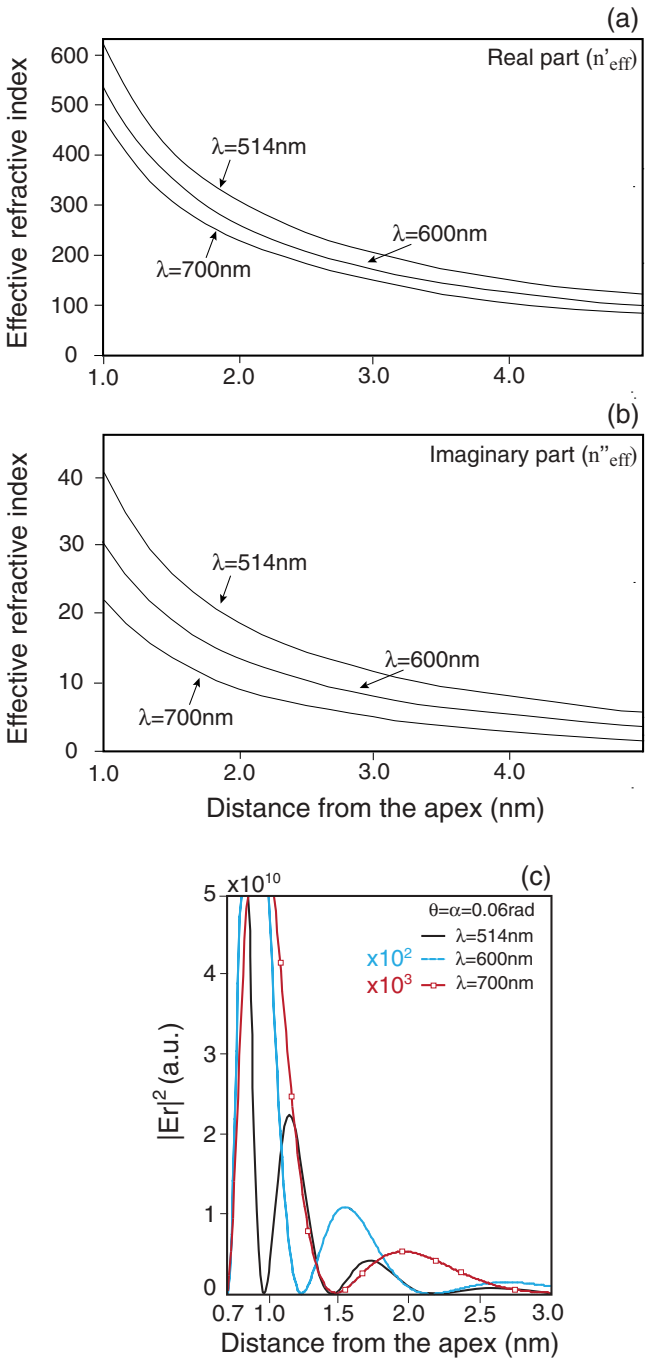

FIG. 7. (Color online) Comparison of the real (a) and imaginary (b) part of the effective refractive index by changing the wavelength of the incoming radiation. Three values of λ are considered: 514 nm, 600 nm, and 700 nm. At the shortest wavelengths is associated the highest effective index. In all three cases the values are calculated on the cone surface with $\theta = \alpha = 0.06$ rad. (c) Same as in (a) and (b) with the intensity of the electric field along the ordinate.

system is $E_{\text{flat}} \propto e^{-k''_{\text{eff,flat}}x}$, where $k''_{\text{eff,flat}}$ is the wave vector along the interface (x direction) associated with the polariton mode.[16] This expression can be conveniently rewritten in terms of the imaginary part of the effective refractive index $n''_{\text{eff,flat}}$, obtaining $E_{\text{flat}} \propto e^{-(2\pi/\lambda)n''_{\text{eff,flat}}x}$. Obviously, the longer the excitation wavelength λ the lower the absorption and, similarly, the higher $n''_{\text{eff,flat}}$ the stronger the decay. If now we turn our attention back to the conical metallic structures, we can notice what, at first sight, might look like a strange behavior. In fact, in Fig. 7(c) the highest field, namely the one with the lowest QA, is associated with both the lowest wavelength and the highest n''_{eff}. This reading contradicts the previous description of surface plasmon polaritons on a flat metallic-dielectric interface; that is, the absorptions of the two systems show opposite trends. In order to understand this important aspect we have to explicitly relate the field E_r to the effective refractive index. In particular, E_r depends on the imaginary part n''_{eff} through the quantity $e^{-(\omega/c)n''_{\text{eff}}r\ln(r)}$ which is directly obtained from Eq. (3), with

$$\eta' = \frac{\omega}{c}n'_{\text{eff}}r, \quad \eta'' = \frac{\omega}{c}n''_{\text{eff}}r.$$

It is only formally similar to the well-known relation $e^{-(\omega/c)n''_{\text{eff,flat}}x}$ valid for SPP on a flat interface where any increase of $n''_{\text{eff,flat}}$ determines a stronger absorption. The difference between the two cases can be well explained by noticing that the presence of the term $\ln(r)$ increases the value of the function associated with the highest n''_{eff} according to a behavior which is opposite from what is observed on a flat interface (the higher is $n''_{\text{eff,flat}}$ the stronger is the decay). To better understand this point we shall write Eq. (3) in terms of n_{eff}:

$$R(r) \propto r^{-1/2}\cos\left(\frac{\omega}{c}n'_{\text{eff}}r\ln r\right)(e^{(\omega/c)n''_{\text{eff}}r\ln r} + e^{-(\omega/c)n''_{\text{eff}}r\ln r})$$
$$\sim r^{-1/2}\cos\left(\frac{\omega}{c}n'_{\text{eff}}r\ln r\right)(e^{-(\omega/c)n''_{\text{eff}}r})^{\ln r}.$$

The last approximation is valid for $r < 1$ (similarly, if $r > 1$ the quantity $e^{(\omega/c)n''_{\text{eff}}r\ln r}$ would have been taken into account) and allows a direct comparison with the solution of a metal-dielectric interface $e^{-(\omega/c)n''_{\text{eff,flat}}r}$ which shows the crucial role played by the exponent $ln(r)$ in case of a metallic conical structure. In Fig. 8(a) we have plotted the quantity E_r for two cases: (a) n''_{eff} was considered; (b) n''_{eff} was neglected. The following equations describe these situations:

$$E_{r,n''_{\text{eff}}\neq 0,\theta=\alpha} = -\frac{2ic}{\omega\epsilon_{m,d}}\frac{\eta A_{1,2}}{r^{3/2}}I_0(\eta\alpha)\cos\left(\frac{\omega}{c}n'_{\text{eff}}r\ln r\right)$$
$$\times 2\cosh\left(\frac{\omega}{c}n''_{\text{eff}}r\ln r\right) + \text{c.c.},$$

$$E_{r,n''_{\text{eff}}\to 0,\theta=\alpha} = -\frac{2ic}{\omega\epsilon_{m,d}}\frac{\eta A_{1,2}}{r^{3/2}}I_0(\eta\alpha)\cos\left(\frac{\omega}{c}n'_{\text{eff}}r\ln r\right)$$
$$+ \text{c.c.}$$

The result shows how the presence of n''_{eff} *increases* the value of E_r (that is, reduces QA) and this effect is stronger the closer to the tip apex. For example, at $r = 1.75$ nm there are more than three orders of magnitude difference between the two cases. This explains the higher value of E_r for $\lambda = 514$ nm when compared to $\lambda = 600$ nm and $\lambda = 700$ nm. A strong message rises from this achievement: The term *absorption* cannot be associated with the imaginary part of the *effective* refractive index when dealing with conical nanometric size metallic structures.

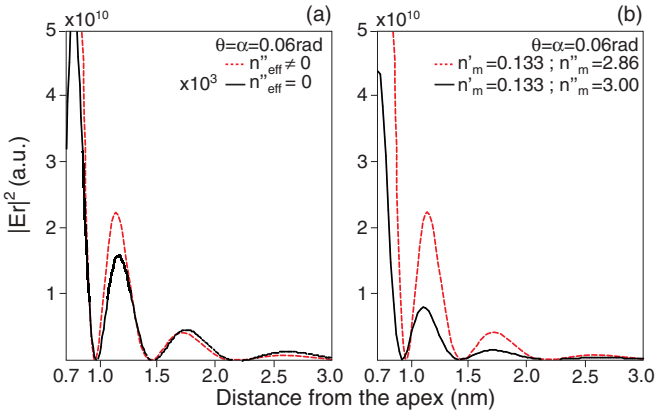

FIG. 8. (Color online) Polaritonic field traveling on a metallic conical surface ($\theta = \alpha$). Two situations are shown: (a) field in terms of *effective* refractive index; (b) field in terms of *metal bulk* refractive index. The former shows an increase of the field when n''_{eff} is increased. The latter shows an opposite behavior: decrease of the field when n''_m is increased. For both cases $\lambda = 514$ nm and $\theta = \alpha = 0.06$ rad were considered.

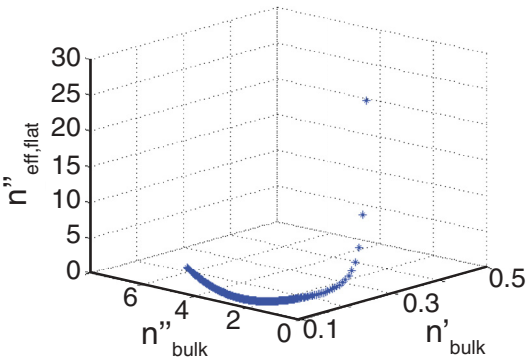

FIG. 9. (Color online) The effective refractive index $n''_{\text{eff,flat}}$ for a silver-air flat interface is plotted in terms of the bulk values of the refractive index. A nonmonotonic behavior is found.

Now we shall proceed showing the role played by the *metal bulk* value of the refractive index and whether its imaginary part can be associated with absorption (i.e., QA) in the case of conical metallic structures. The plots in Fig. 8(b) show the two cases with bulk $\epsilon_m = -8.19 + i0.760$ and $\epsilon_m = -8.98 + i0.798$. They correspond to the bulk refractive indexes $n_m = 0.133 + i2.86$ and $n_m = 0.133 + i3.00$, respectively. The result is very clear: the higher the imaginary part of the bulk refractive index, the lower the electric field. Hence, the canonical meaning of absorption associated with the imaginary part of the refractive index is recovered when dealing with *bulk* refractive index.

Finally an observation on flat metal-dielectric interfaces. As we have previously seen the electric field contribution along the interface (here the x direction) can be written as $E_{\text{flat}} \propto e^{-(\omega/c)n''_{\text{eff,flat}}x}$. This expression states that the higher is $n''_{\text{eff,flat}}$ the stronger is the absorption. If now we relate the quantity $n''_{\text{eff,flat}}$ to the bulk values of the refractive index, we can conclude that it is not straightforward to asset that an increase of the *bulk* imaginary part of the refractive index would determine a decrease of the field amplitude. In fact, it is the combination of both the real and imaginary parts of the bulk refractive index which determine the behavior of $n''_{\text{eff,flat}}$. To visualize this concept we have plotted $n''_{\text{eff,flat}}$ as a function of n'_{bulk} and n''_{bulk} when a flat silver-air interface was considered (see Fig. 9). In other words, before assuming that an increase of the imaginary part of the refractive index automatically implies an increase of the absorption, considerations on the nature of the field have to be made.

We conclude this section by noticing that the wavelength dependence of the field along the surface of the metallic cone is opposite of that obtained when the field is calculated away (in the surrounding dielectric) from the tip apex. In fact, the latter shows an increase of the field with the wavelength.[24] This can be explained by noticing that a realistic cone shows a tip end which can be described by a semi-nanosphere with a few nanometers radius. Under radially polarized light (such as a TM_0 mode) the light reaching the cone apex creates a local dipole oriented along the cone axis whose radiation intensity is proportional to the wavelength λ.

V. DISPERSION RELATION

The dependence of the TM_0 refractive index n'_{eff} on both the wavelength λ and the distance from the cone apex r is summarized by the dispersion relation $\omega(k'_{\text{eff}})$ of Fig. 10(a), being $k_{\text{eff}} = k'_{\text{eff}} + ik''_{\text{eff}} = \frac{\omega}{c}(n'_{\text{eff}} + in''_{\text{eff}})$. The figure shows that the higher the radial distance r the steeper the dispersion curve. This is in agreement with the fact that in the limit of $r \to 0$ the velocity of the polaritonic field tends to zero, namely $\frac{d\omega}{dk} = 0$. Furthermore, the dispersion relation of the HE_1-like mode numerically calculated[22] in proximity to the tip apex is also plotted. In fact, when a metallic conical structure is illuminated with a linearly polarized source, both the TM_0 and HE_1-like modes are generated.[23,24] The figure shows no intersecting points between the two modes' dispersion curves, meaning that the modes travel independently on the cone without any mode conversion occurring.[25] Finally, Fig. 10(b) shows the comparison between the HE_1-like mode on a conical structure and a TM mode on a flat silver-air interface. The result indicates that the HE_1-like mode propagates on the conical structure in a manner very similar to that of the TM mode on a flat interface; however the former, in the limit of $r \to 0$, can directly couple to the external radiation by becoming a radiative mode.

In order to sustain this statement, the interaction between a silver conical structure and an electromagnetic wave ($\lambda = 633$ nm) with two different angles of incidence has been numerically simulated with commercial FEM software.[26] The cone is 1250 nm long and the base diameter is 150 nm, which means an idealized half-apex angle $\alpha = 0.06$ rad. The cone end was then adjusted in order to realize a numerical simulation resembling as much as possible experimental conditions; in fact it was modified to show an apex radius of curvature of 5 nm.[21] Figure 11(a) shows the ratio $U = (|E(37^\circ)| - |E(0^\circ)|)/(|E(37^\circ)| + |E(0^\circ)|)$ calculated on the edge of the cone (from the base to the apex) generated by a linearly TEM polarized wave propagating with an angle from the cone axis of either 37° or 0° (a 0° angle of incidence corresponds to a propagation direction parallel to the axis of the cone). As

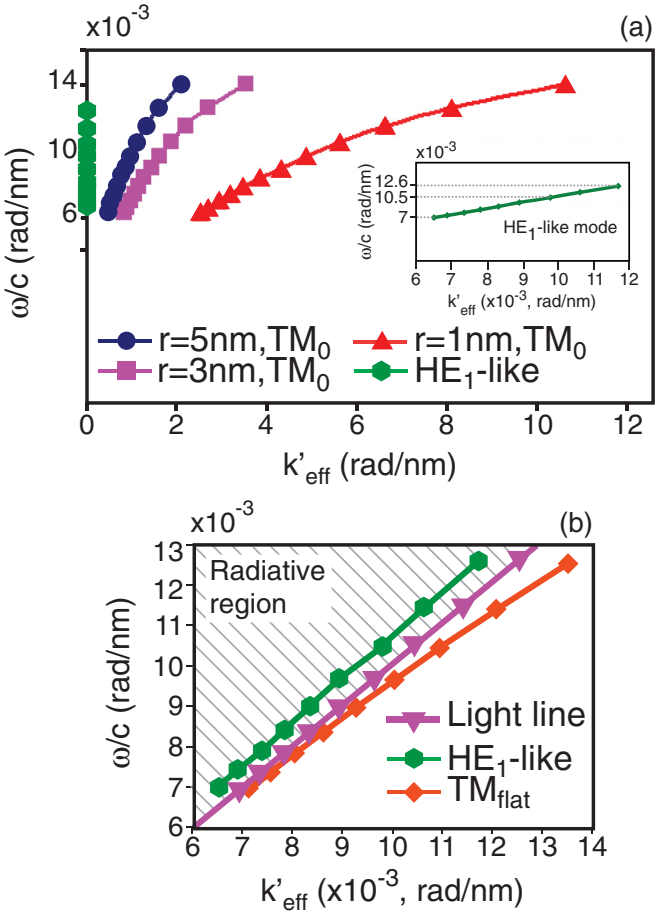

FIG. 10. (Color online) (a) Dispersion relation for a conical structure by changing the distance r from the cone apex along the cone surface. In particular, three values of r are considered: $r = 1$ nm, $r = 3$ nm, and $r = 5$ nm. Furthermore, the comparison between the TM_0 and HE_1-like modes traveling on the cone is shown. The inset shows the HE dispersion curve on a larger scale. The HE_1-like and TM_0 dispersion curves do not intersect each other for any value of k'_{eff}. (b) Direct comparison between an HE_1-like mode traveling on a silver cone and a TM mode traveling on a silver flat surface. The light line *in vacuo* is also plotted together with the radiative region (dashed area).

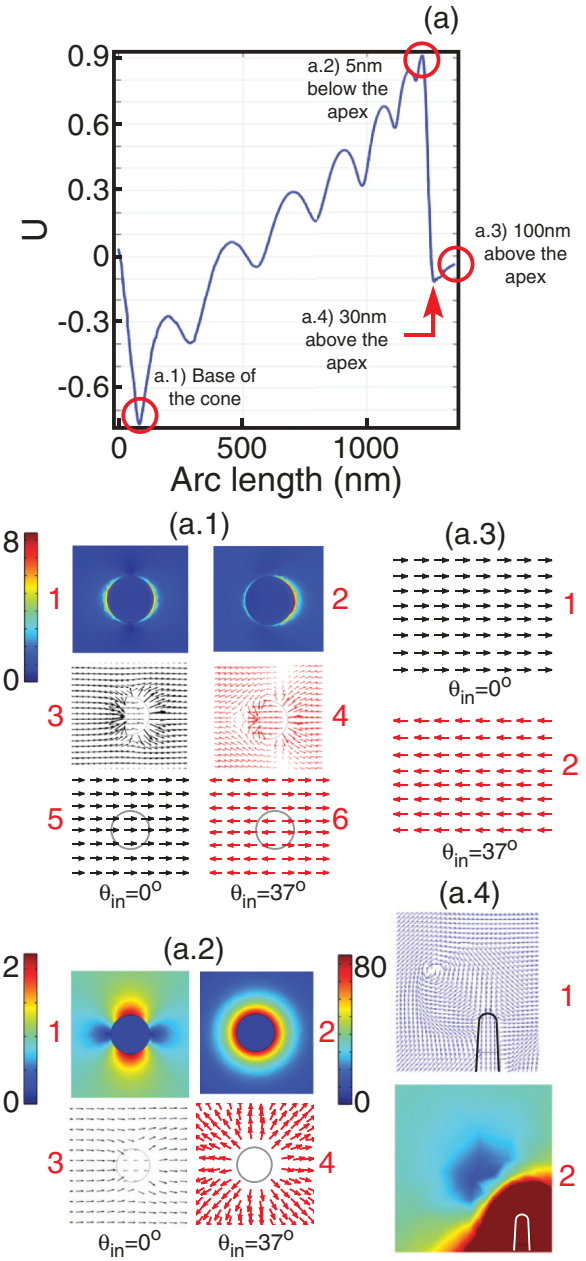

FIG. 11. (Color online) (a) The U profile along the cone edge is plotted. (a.1) Panels 1, 2: Norm of *total* (incident + scattered) electric field for the excitation wave at angle θ_{in} equal to 0° and 37°, respectively. Panels 3, 4: Vectorial *total* electric field representation for the 0° and 37° excitation waves, respectively. Panels 5, 6: Vectorial *incident* electric field representation for the 0° and 37° excitation waves, respectively. (a.2) Scalar and vectorial representation of the *total* electric field calculated for excitation waves at 0° and 37°. The TM_0 and HE_1-like mode shapes are easily recognized. (a.3) *Total* vectorial field calculated 100 nm above the cone tip for the two excitation angles 0° and 37°. (a.4) Panel 1: Poynting vector around the cone tip. Panel 2: Norm of the total electric field. Both figures refer to a 37° excitation wave. Above the apex the total field drops below the excitation amplitude. The phase of the optical field is undefined and the Poynting vector goes to a vortex-like shape.

recently pointed out,[24] whereas at 0° the incident TEM source cannot induce the generation of a TM_0 mode in the cone, tilting the source (e.g., at 37°) allows adiabatic compression. In fact in Fig. 11(a) we clearly see that at the apex of the cone almost the totality of the field intensity is given by the tilted wave ($U = 0.9$). At this spot the field is given by an almost pure TM_0 mode as shown in Fig. 11(a.2) (right side, compare the scale bars). On the other hand, a 0° wave does not give substantial enhancement and the mode is HE-like all along the cone [Fig. 11(a.2), left side]. When we look at 100 nm outside the apex, a TM_0 mode cannot be sustained in any case and U approaches a value around zero as shown in Fig. 11(a.3). The fact that just above the cone tip U becomes negative in a small interval of space can be explained in terms of destructive interference between incident and scattered field giving rise to phase singularities[27,28] [Fig. 11(a.4)]. We can notice that U becomes negative also near the base of the cone. Intuitively we might expect U to be around zero at the base where the dispersion relation is linear for the 0° wave and compression is

not formed yet for the 37° one. The fact is that the 0° incident wave couples with the base of the cone giving rise to a sensitive enhancement at the edge of the structure [Fig. 11(a.1), left side]; the tilted wave (37°) produces the same effect but the phase difference in the incident field lowers the signal and U goes below zero [Fig. 11(a.1)].

VI. RAMAN MEASUREMENTS

A cone with the same geometrical characteristics as in Fig. 1 was also fabricated. In particular, it was embedded in a photonic crystal cavity[29–31] in order to enhance the coupling efficiency with the external radiation.[15,21] Two fabrication techniques were implemented: focused ion beam (FIB) milling[32–34] to produce the photonic crystal and chemical vapor deposition (CVD) induced by focused electron beam to grow the metallic conical structure on top of the photonic crystal. The results of the nanofabrication process are shown in Fig. 12. A monolayer of benzenethiol was deposited, via chemisorption technique, over silver-based nanocones with a different radius of curvature (RoC) at the apex, from 30 nm to 10 nm. The same procedure of monolayer deposition and the same Raman measurement parameters were employed for all the structures. In particular, the measurements were taken right after the fabrication of the device to limit the effects originating by the silver oxidation. Moreover, the sample was kept in a nitrogen environment to prevent an additional absorption of reactive species such as sulfur and oxygen. It is found that for the nanocone with RoC 30 nm the chemical information of the substance under investigation is not revealed because of the low field enhancement. However, by lowering the nanocone RoC the vibrational bands of the molecule start emerging, showing the molecular chemical information, in accordance with the theoretical behavior shown in Figs. 2 and 3. The SPPERS spectra associated with the benzenethiol monolayer deposited on the nanocones with different RoC are shown in Fig. 13(a). Furthermore, wavelength response comparison was carried out on a quantum dot (QD) deposited at the tip

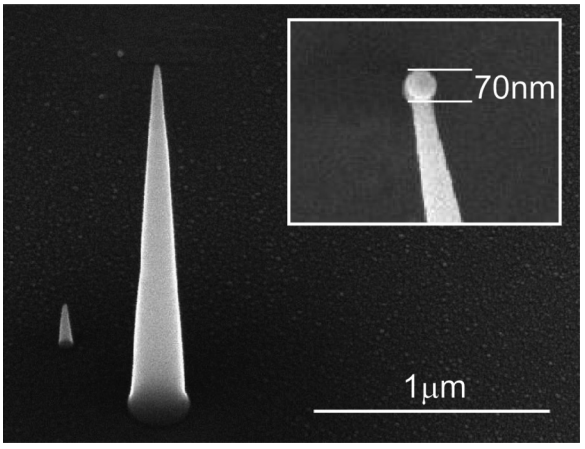

FIG. 12. SEM image of a nanocone fabricated on a silicon nitride membrane by means of the electron beam induced deposition technique. The nanocone height is about 2 μm, the base is 280 nm, and the radius of curvature of the tip is below 5 nm. The inset shows a similar situation when a particle of SiO_x is deposited on the tip.

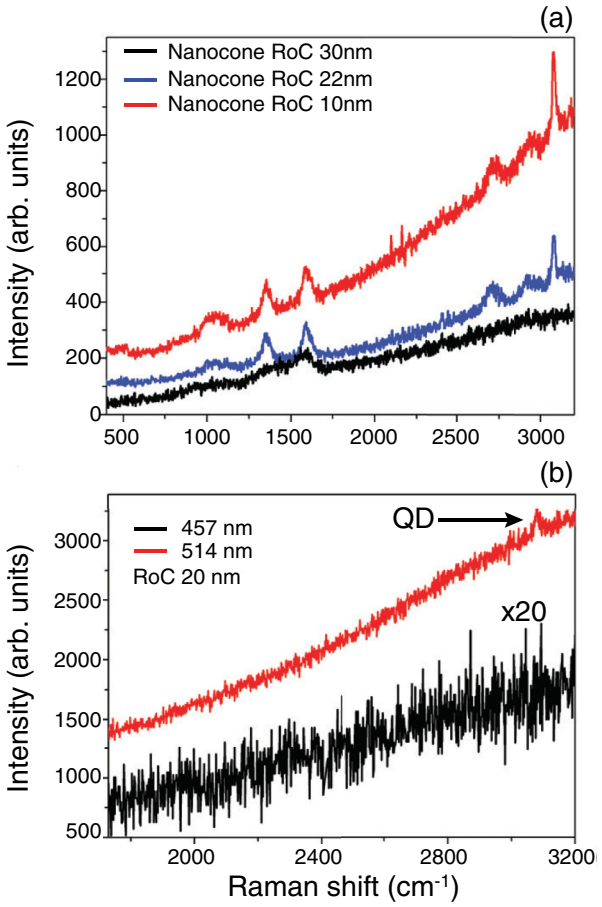

FIG. 13. (Color online) (a) SPPERS spectra coming from a layer of benzenethiol deposited on conical silver structures with three different RoC's. In all the experiments we used a 150× objective lens with power source equal to 0.09 mW, an accumulation time of 100 sec, and an excitation wavelength equal to 514 nm. This wavelength was chosen to provide the highest possible enhancement as shown in Fig. 7. (b) Raman response on a QD deposited on a 20 nm RoC tip when 457 nm and 514 nm excitation sources were considered.

end of a 20 nm RoC tip. The utilized wavelengths are 457 nm and 514 nm as shown in Fig. 13(b). In particular, only the 514 nm excitation was able to provide enough intensity in order to resolve the QD peak at 3070 cm^{-1}. This result is in agreement with the previously discussed dipole-like behavior of the present tips.

Similar measurements were also performed on a 35 nm radius bead of SiO_x deposited on a nanocone, as shown in the inset of Fig. 12. The strong position dependence of the Raman signal has been verified by SPPERS measurements. It is very important to point out that SiO_x has very low scattering cross section, showing low Raman signal from the bulk. However, regarding the enhancement properties of our device, even a very small amount of SiO_x on the tip of the nanocone was able to produce a very clear Raman signal, as shown in Fig. 14. In fact the figure presents a very well defined peak centered around 450 cm^{-1} and as large as 300 cm^{-1}.

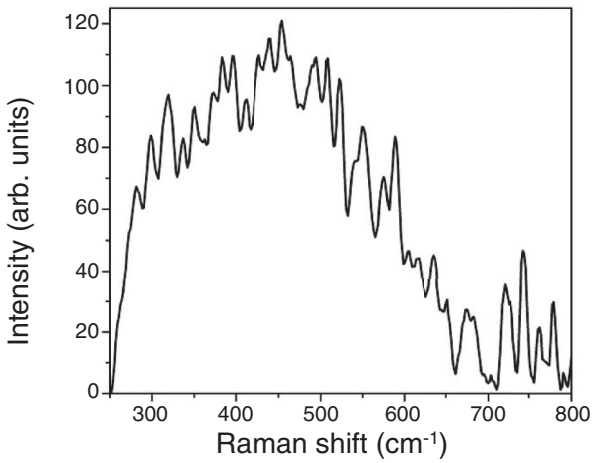

FIG. 14. SPPERS spectra coming from a bead of SiO_x deposited on a metallic conical tip with RoC = 10 nm. The excitation wavelength and the power source were 514 nm and 0.18 mW, respectively.

VII. SUMMARY

In conclusion, we have simulated and fabricated a nano-optic polaritons-based device showing adiabatic properties which was utilized for surface plasmon polaritons enhanced Raman spectroscopy (SPPERS) measurements. We have introduced a fully analytical model describing both the adiabatic compression and the physical role played by the complex refractive index for a metallic conical structure. In particular, the role of the absorption on the field enhancement was investigated. Furthermore, illuminating the device with a linearly polarized light can develop an HE_1 mode that, in proximity to the tip apex, shows radiative characteristics (above the light line) which do not allow energy exchange with the adiabatic TM_0 mode. Finally, we have illustrated how the tip at nanoscale level can play a very important role for the determination of Raman peaks otherwise absent under more canonical micro-Raman investigation. The measurements were performed on two kinds of samples: a monolayer of benzenethiol and a 35 nm radius SiO_x bead. They were both deposited on the nanocone structure; in particular the former was extensively covering the cone surface whereas the latter was localized only on its apex. In both cases clear SPPERS spectra were achieved due to the giant electric field enhancement induced by the geometrical characteristics of the cone, as theoretically predicted.

ACKNOWLEDGMENTS

We would like to thank Kh. V. Nerkararyan for the very useful and interesting discussion. The authors gratefully acknowledge support from European Projects SMD FP7-NMP-2008-SMALL-2, Proposal No. CP-FP 229375-2 and Nanoantenna FP7-HEALTH-2009, Grant No. 241818; FOCUS FP7 No. 270483.

*remo.proietti@iit.it

[1] A. J. Babadjanyan, N. L. Margaryan, and Kh. V. Nerkararyan, J. Appl. Phys. **87**, 3785 (2000).
[2] M. I. Stockman, Phys. Rev. Lett. **93**, 137404 (2004).
[3] W. Zhang, X. Cui, and O. J. F. Martin, J. Raman Spectrosc. **40**, 1338 (2009).
[4] L. Vaccaro, L. Aeschimann, U. Staufer, H. P. Herzig, and R. Dändliker, Appl. Phys. Lett. **83**, 584 (2003).
[5] N. A. Issa and R. Guckenberger, Plasmonics **2**, 31 (2007).
[6] Kh. V. Nerkararyan, A. A. Hakhoumian, and A. E. Babayan, Plasmonics **3**, 27 (2008).
[7] C. Nobile, V. A. Fonoberov, S. Kudera, A. Della Torre, A. Ruffino, G. Chilla, T. Kipp, D. Heitmann, L. Manna, R. Cingolani, A. A. Balandin, and R. Krahne, Nano Lett. **7**, 476 (2007).
[8] G. Das, F. Mecarini, F. Gentile, F. De Angelis, M. Kumar, P. Candeloro, C. Liberale, G. Cuda, and E. Di Fabrizio, Biosens. Bioelectron. **24**, 1693 (2009).
[9] M. L. Coluccio, G. Das, F. Mecarini, F. Gentile, L. Bava, R. Tallerico, P. Candeloro, C. Liberale, F. De Angelis, and E. Di Fabrizio, Microelectron. Eng. **86**, 1085 (2009).
[10] F. De Angelis, F. Gentile, F. Mecarini, G. Das, M. Moretti, P. Candeloro, M. L. Coluccio, G. Cojoc, A. Accardo, C. Liberale, R. Proietti Zaccaria, G. Perozziello, L. Tirinato, A. Toma, G. Cuda, R. Cingolani, and E. Di Fabrizio, Nat. Photon. **5**, 682 (2011).
[11] J. Miragliotta and T. E. Furtak, Phys. Rev. B **35**, 7382 (1987).
[12] P. Corio, S. D. M. Brown, A. Marucci, M. A. Pimenta, K. Kneipp, G. Dresselhaus, and M. S. Dresselhaus, Phys. Rev. B **61**, 13202 (2000).
[13] T. J. Davis, D. E. Gomez, and K. C. Vernon, Phys. Rev. B **82**, 205434 (2010).
[14] P. I. Geshev, U. Fischer, and H. Fuchs, Phys. Rev. B **81**, 125441 (2010).
[15] F. De Angelis, M. Patrini, G. Das, I. Maksymov, M. Galli, L. Businaro, L. C. Andreani, and E. Di Fabrizio, Nano Lett. **8**, 2321 (2008).
[16] H. Raether, in *Surface Plasmons* (Springer-Verlag, Berlin, Heidelberg, 1988).
[17] S. A. Maier, in *Plasmonics* (Springer, New York, 2007).
[18] CST Microwave Studio 2010 [http://www.cst.com].
[19] A. D. Rakic, A. B. Djuriic, J. M. Elazar, and M. L. Majewski, Appl. Opt. **37**, 5271 (1998).
[20] P. A. Belov, R. Marqués, S. I. Maslovski, I. S. Nefedov, M. Silveirinha, C. R. Simovski, and S. A. Tretyakov, Phys. Rev. B **67**, 113103 (2003).
[21] F. De Angelis, G. Das, P. Candeloro, M. Patrini, M. Galli, A. Bek, M. Lazzarino, I. Maksymov, C. Liberale, L. C. Andreani, and E. Di Fabrizio, Nat. Nanotech. **5**, 67 (2010).
[22] CST Microwave Studio was used for the approximative calculation of the HE_1 effective refractive index. In particular, it was determined through the estimation of the effective wavelength λ_{eff} of the mode calculate at a distance $r \sim 1$ μm from the tip apex ($cR \sim 60$ nm). Considering shorter values of r than 1 μm would have the effect of increasing λ_{eff}; namely the HE_1 dispersion curve would move even more inside the radiative region of the dispersion curve graph [see Fig. 10(b)].
[23] F. De Angelis, R. Proietti Zaccaria, M. Francardi, C. Liberale, and E. Di Fabrizio, Opt. Express **19**, 22268 (2011).

[24]R. Proietti Zaccaria, F. De Angelis, A. Toma, L. Razzari, A. Alabastri, G. Das, C. Liberale, and E. Di Fabrizio, Opt. Lett. **37**, 545 (2012).
[25]J. Song, R. Proietti Zaccaria, G. Dong, E. Di Fabrizio, M. B. Yu, and G. Q. Lo, Opt. Express **19**, 25206 (2011).
[26]COMSOL Multiphysics [http://www.comsol.com].
[27]H. F. Schouten, T. D. Visser, and D. Lenstra, J. Opt. B **6**, S404 (2004).
[28]S. V. Boriskina and M. R. Bjorn, Nanoscale **4**, 76 (2011).
[29]J. F. Song, R. Proietti Zaccaria, M. B. Yu, and X. W. Sun, Opt. Express **14**, 8812 (2006).
[30]R. Proietti Zaccaria, P. Verma, S. Kawaguchi, S. Shoji, and S. Kawata, Opt. Express **16**, 14812 (2008).
[31]M. Galli, M. Agio, L. C. Andreani, L. Atzeni, D. Bajoni, G. Guizzetti, L. Businaro, E. Di Fabrizio, F. Romanato, and A. Passaseo, Eur. Phys. J. B **27**, 79 (2002).
[32]S. Cabrini, A. Carpentiero, R. Kumar, L. Businaro, P. Candeloro, M. Prasciolu, A. Gosparini, C. Andreani, M. De Vittorio, T. Stomeo, and E. Di Fabrizio, Microelectron. Eng. **78**, 11 (2005).
[33]S. Cabrini, R. J. Barsotti, A. Carpentiero, L. Businaro, R. Proietti Zaccaria, F. Stellacci, and E. Di Fabrizio, J. Vac. Sci. Technol. B **23**, 2806 (2005).
[34]F. Schiappelli, R. Kumar, M. Prasciolu, D. Cojoc, S. Cabrini, M. De Vittorio, G. Visimberga, A. Gerardino, V. Degiorgio, and E. Di Fabrizio, Microelectron. Eng. **73**, 397 (2004).